coatings

MDPI

Article

ZnS:Cu/PDMS Composite Coating for Combating Marine Biofouling

Zhenze Liu [1], Yicong Zhang [2], Tianyi Wang [3], Wenbo Du [4,*] and Huichao Jin [2,*]

[1] College of Communication Engineering, Jilin University, Changchun 130012, China; zzliu@jlu.edu.cn
[2] Key Laboratory of Bionic Engineering, Ministry of Education, Jilin University, Changchun 130022, China; yicong23@mails.jlu.edu.cn
[3] State Key Laboratory of Superhard Materials, Jilin University, Changchun 130012, China; tywang22@mails.jlu.edu.cn
[4] National Key Laboratory for Remanufacturing, Army Academy of Armored Forces, Beijing 100072, China
* Correspondence: dwbneu@163.com (W.D.); jinhc@jlu.edu.cn (H.J.)

Abstract: Biofouling is a major concern in marine industries. The use of traditional toxic antifouling coatings is forbidden or severely restricted. This study aimed to provide a green and effective antifouling coating. The coating was prepared using a polydimethylsiloxane (PDMS) matrix and Cu-doped zinc sulfide (ZnS:Cu). Four samples with different ZnS:Cu contents (1, 10, 20, and 50 wt%) were prepared. Pristine PDMS (0 wt%) was used as the control. The results showed that all coatings had hydrophobic surfaces conducive to combating biofouling. In tests against *B. Subtilis*, the 1, 10, 20, and 50 wt% samples showed enhanced antifouling capabilities compared to the 0 wt% sample. In static and dynamic tests against *Chlorella*, the antifouling capability increased with increasing ZnS:Cu content and the 50 wt% sample showed the best antifouling capability. The possible antifouling mechanisms of these coatings include the release of ions (Zn^{2+} and Cu^{+}), induction of deformation, and fluorescence emission. This study provides a reference for the application of Zn^{2+}/Cu^{+} combinations to combat marine biofouling.

Keywords: PDMS; cuprous oxide; zinc ion; marine biofouling; antifouling coating

check for updates

Citation: Liu, Z.; Zhang, Y.; Wang, T.; Du, W.; Jin, H. ZnS:Cu/PDMS Composite Coating for Combating Marine Biofouling. *Coatings* **2023**, *13*, 2083. https://doi.org/10.3390/coatings13122083

Received: 15 November 2023
Revised: 12 December 2023
Accepted: 13 December 2023
Published: 14 December 2023

Copyright: © 2023 by the authors. Licensee MDPI, Basel, Switzerland. This article is an open access article distributed under the terms and conditions of the Creative Commons Attribution (CC BY) license (https://creativecommons.org/licenses/by/4.0/).

1. Introduction

Biofouling of marine vessels can increase the surface roughness, leading to increased drag resistance and fuel consumption [1]. Biofouling accelerates surface corrosion and affects equipment safety; therefore, it is a major issue in the marine industry [2]. Traditional antifouling coatings contain toxic chemicals such as mercury, arsenic, and tributyltin (TBT). Although these toxic coatings are effective in combating biofouling, they exhibit teratogenic and lethal effects on other marine organisms. Their most serious consequence is that they can harm human health by bioaccumulating in food chains. Several countries have reported the presence of TBT in humans [3,4]. In 2001, the International Maritime Organization (IMO) passed a ban on the application of TBT by 1 January 2003, and a total ban on the use of TBT by 1 January 2008. Therefore, it is necessary to develop environmentally friendly and effective antifouling coatings.

Biofouling is a stepwise process that involves the formation of a conditioning film, a biofilm, and macroscopic fouling [5]. Preventing biofilm formation (where the major contributors are bacteria and diatoms) can inhibit the subsequent biofouling stages [1]. Recently, several metal ions, including zinc (Zn^{2+}), copper (Cu^{+} and Cu^{2+}), and silver (Ag^{+}) ions, have been used to combat biofouling because of their microbial activity [6,7]. The toxicity of these metal ions (e.g., Cu) is lower than that of TBT, and they are considered relatively green antifouling biocides under government supervision and approval [8,9]. Pristine or modified metal ions are mostly used as fillers to enhance the antifouling capabilities of coatings. For example, silicone/ZnO nanorod composite coating [10], ZnO/multi-walled

carbon nanotube/polyethersulfone composite coating [11], polyhexanide-coated copper oxide nano-particles/poly (vinylidene fluoride) composite coating [12], cuprous oxide microcapsule/polyvinylpyrrolidone antifouling coating [13], AgNPs/poly(di(ethylene glycol)methyl ether methacrylate) coating [14], Ag@TA-SiO_2 nanospheres/terpolymer coating [15], and Ag/ polydimethylsiloxane (PDMS) composite coating [16] have shown potential for preventing marine biofouling. However, most of these solutions involved a single metallic ion. A recent study showed that a single metal-based coating has antifouling limitations (e.g., limited broad-spectrum antifouling capability and durability) under various conditions [17]. Therefore, combining metal ions with other materials to fabricate synergistic antifouling coatings has attracted the attention of researchers. Tian et al. reported a Cu-Ti composite coating by plasma spraying of mechanically mixed Cu/Ti powders, and the coating showed remarkable antifouling efficiency against bacterial survival and adhesion up to ~100% [18]. Calabrese et al. investigated the synergistic effects of Cu, Ag, and titanium dioxide (TiO_2) [19]. The Cu/TiO_2 powder exhibited the best antifouling performance due to its synergistic effect. Recently, many metallic-ion combinations, including ZnO/Fe_2O_3 [20], graphene/Ag [21], g-C_3N_4/ZnO [22], and Cu/TiO_2 [23] have exhibited enhanced antifouling capabilities.

To the best of our knowledge, no previous studies have investigated the antifouling capabilities of the Zn^{2+}/Cu^{+} combinations. Cu-doped zinc sulfide (ZnS:Cu) is a semiconductor material that emits luminescence under mechanical forces [24]. In this study, ZnS:Cu was incorporated into polydimethylsiloxane (PDMS) as a filler to investigate the synergistic antifouling effects of Zn^{2+} and Cu^{+}. PDMS is an elastic material that can undergo deformation under the impact of water flow; thus, the ZnS:Cu/PDMS composite coating can emit luminescence in flowing water. Several studies have revealed that luminescence can inhibit algal settlement [25–27]; hence, the ZnS:Cu/PDMS composite coating has double antifouling effects, that is, microbial activity (Zn^{2+}/Cu^{+}) and luminescent drive effects. In the antifouling tests, *Bacillus Subtilis* (*B. Subtilis*) and *Chlorella* were selected as fouling models to evaluate the antifouling capabilities of the ZnS:Cu/PDMS composite coatings.

2. Materials and Methods

2.1. Materials

Commercial ZnS:Cu (model: D502CT, particle size: 25 μm) was purchased from Shanghai Keyan Phosphor Technology Co. Ltd. (Shanghai, China). Two-part PDMS (SYLGARD 184 Silicone Elastomer Kit) was provided by the Dow Corning Corporation (Midland, TX, USA), and the kit included a PDMS base and curing agent. The bacterial strain *B. subtilis* NCIB3610 was provided by Chuanxiang Biotechnology, Co., Ltd. (Shanghai, China). *Chlorella* was provided by HEALTH BIOTECH, Co., Ltd. (Nanjing, China).

2.2. Preparation of ZnS:Cu/PDMS Coating

Method 1: First, 0.25 g of ZnS:Cu, 25 g of PDMS, and 2.5 g of the curing agent were mixed for 5 min using a mechanical stirrer at 80 rpm. The mixture was then placed in a vacuum oven at room temperature to remove internal bubbles. When no bubbles overflowed, the mixture was poured into an acrylic model (groove depth = 1 mm). After 48 h of curing at room temperature, a 1 wt% ZnS:Cu/PDMS coating was obtained.

Method 2: Because micro- and nano-particles have a high specific surface per unit volume, they exhibit high surface free energies (SFEs) [28]. It is difficult to distribute these particles uniformly in a low-surface-energy polymer matrix (e.g., silicone and fluorine polymers) due to the differences in their SFEs. Additionally, micro- and nano-particles are affected by gravity. Hence, during curing, the particles tend to move toward the bottom of the composite material. Therefore, the ZnS:Cu/PDMS coating prepared using Method 1 may have limitations in terms of dispersibility. A new preparation method was used to address this issue as follows:

First, 25 g of PDMS and 2.5 g of the curing agent were mixed for 5 min using a mechanical stirrer at 80 rpm, and the mixture was placed in a vacuum oven at room

temperature to remove the internal bubbles. The mixture was allowed to stand in air for *A* hours to increase its viscosity, after which 0.25 g of ZnS:Cu was added and stirred for 30 min. The ZnS:Cu/PDMS mixture was poured into an aluminum alloy model (groove depth = 1 mm) and placed in a vacuum oven to remove the internal bubbles. The model was then placed on a heating platform under *B* °C for *C* mins. After curing, a 1 wt% ZnS:Cu/PDMS coating was prepared. In addition, 10, 20, and 50 wt% ZnS:Cu/PDMS samples were prepared, and pristine PDMS (0 wt%) was used as the control group. Based on our experience, the viscosity after 5–8 h was accepted for preparation. According to the technical data sheet of SYLGARD 184 Silicone Elastomer, the curing time of PDMS at 25, 100, 125, and 150 °C are 28 h, 35 min, 20 min, and 10 min, respectively. Considering the effects of incorporated ZnS:Cu particles and coating thickness, the curing parameters of 80 °C (240 min) and 150 °C (20 min) were used. The parameter combinations for *A*, *B*, and *C* are listed in Table 1.

Table 1. Three preparation methods.

Group	*A* (h)	*B* (°C)	*C* (min)
1	5	80	240
2	7	80	240
3	8	150	20

2.3. Characterization Analysis

Water contact angles (WCA) were measured using a drop shape analyzer (DSA25, Kruss, Hamburg, Germany). In the WCA measurement, a 5.0 µL deionized (DI) water droplet was applied, and each sample was measured five times to reduce experimental error. The SFEs were estimated using Equation (1) [29]:

$$\cos\theta = -1 + 2\sqrt{\frac{\gamma_S}{\gamma_L}}\left[1-\beta\left(\gamma_L-\gamma_S\right)^2\right] \quad (1)$$

where θ is the WCA and γ_S and γ_L are the SFEs of solid and liquid, respectively. β can be considered a constant with the value of 1.129×10^{-4} m^2/mJ. The γ_L of DI water is 72.8 mJ/m^2. Surface chemical state information was analyzed using an X-ray photoelectron spectrometer (XPS, ESCALAB 250XI, ThermoFisher Scientific, Waltham, MA, USA) with Al Ka x-rays. The chemical groups of the samples were analyzed using a Fourier-transform infrared (FT-IR) spectrometer (Nicolet iS10, Thermo Scientific, Waltham, MA, USA). The ZnS:Cu sample for the FT-IR measurements was prepared using the KBr pellet method, and the thickness of the prepared sample was tens of microns. The surface elements were measured using an energy-dispersive spectrometer (EDS, HORIBA EMAX, HORIBA, Ltd., Kyoto, Japan). Tensile tests were performed using a tensile tester (UTM5305, YOUHONG, Shanghai, China), and the reference measurement procedure was GB/T 528-2009 [30]. To test the weight loss of the samples in a water environment, the pristine samples were immersed in DI water for 72 h, after which the samples were placed into a vacuum oven at 40 °C for 48 h. After drying, the weight loss of each sample was calculated as follows:

$$\text{Weight loss} = (M_0 - M_1)/M_0 \times 100\% \quad (2)$$

where M_0 is the weight of the pristine sample and M_1 is the weight of the dried sample after immersion.

2.4. Antifouling Tests

Antibacterial Test. The samples were immersed in ethyl alcohol under ultrasonication for 20 min and then dried in a vacuum oven for 1 h. The method for the culture of *B. subtilis* was the same as previously reported [25,31]. The bacterial suspension was diluted to 10^6 CFU/mL. The samples were immersed in the bacterial solution at 37 °C for 24 h.

After the test, the samples were gently washed with phosphate-buffered saline (PBS) to remove unattached bacteria. The samples and PBS were placed in separate centrifuge tubes and ultrasonically cleaned for 5 min to detach the attached bacteria. The PBS and bacteria mixture were then diluted to 10^{-4}. The diluted mixture was evenly deposited on a solid agar medium and cultured for 24 h. Finally, the individual colonies on the plate were counted to determine the antifouling capabilities of the samples. Three parallel experiments were performed for each sample to minimize the experimental error. The antibacterial ratio of each sample was calculated as follows:

$$\text{Antibacterial ratio} = (A - B)/A \times 100\% \quad (3)$$

where A and B are the numbers of bacterial colonies in the control and experimental samples, respectively.

Anti-Algal Settlement Test. The cleaning and bactericidal procedures used for the samples were the same as those described for the antibacterial tests. In the tests under static conditions, the pretreated samples were immersed in a *Chlorella* solution (0.5×10^8 cells/mL) for 15 h. In the tests under dynamic conditions, the samples and *Chlorella* solution were placed in a thermostatic oscillator (SHA-B, JIANGXI RUYU Technology Development Co., Ltd., Shanggao, China) at 150 rpm for 15 h. Because *Chlorella* requires sunlight for photosynthesis, the test was performed under a plant growth lamp (25 W, Hebei Pengxian Agricultural Technology Co., Ltd., Shijiazhuang, China) with a 7.5 h light time and 7.5 h dark periods. After the test, the samples were gently washed with PBS to remove the unattached *Chlorella*. The surface area was measured using a digital microscope (VHX-6000; Keyence, Osaka, Japan). The number of *Chlorella* cells in a 50 μm × 40 μm area was counted to evaluate the antifouling capabilities of the coatings.

3. Results and Discussion

3.1. Preparation Optimization

As shown in Figure 1a, the sample prepared under 48 h curing exhibits obvious double layers. No ZnS:Cu particles can be observed from the top, whereas many ZnS:Cu particles are distributed at the bottom (Figure 1b), and the particle size is approximately 25 μm. Double layers were clearly observed, although the stratification phenomenon was improved in Groups 1 and 2 (Figure 1d,e, respectively). Figure 1f shows a well-prepared coating in which ZnS:Cu is evenly distributed. This stratification phenomenon is primarily attributed to the SFE differences between ZnS:Cu and PDMS, which led to their chemical incompatibility. During the curing process, the ZnS:Cu particles were affected by gravity, leading to the settlement of ZnS:Cu in PDMS (Figure 1c). According to Stokes' law for settling particles, the settling velocity is [32].

$$V = g/18\ ((\rho_s - \rho_f)/\mu)\ D^2 \quad (4)$$

where g is the acceleration due to gravity; ρ_s and ρ_f are the densities of particles and fluid, respectively; μ is the fluid viscosity; and D is the particle diameter. The settling distance is derived as follows:

$$S = Vt \quad (5)$$

where t denotes the settling time. Two strategies are available for reducing the settlement of the ZnS:Cu particles in the PDMS: reducing the settling velocity (V) and reducing the curing time (t). According to Equation (4), V can be decreased by decreasing μ. During the curing process, the viscosity of PDMS increased with increasing time and temperature. Hence, the PDMS/curing agent mixture was allowed to stand in air for several hours to increase the viscosity of the PDMS. Another essential condition is the curing time; particle settlement in the PDMS stops when the PDMS is cured. Therefore, the ZnS:Cu particles in Group 3 (Figure 1f) showed the best dispersibility among the samples. Because particle

dispersibility can affect the performance of the coating, the parameter in Group 3 was a good choice for preparing such coatings.

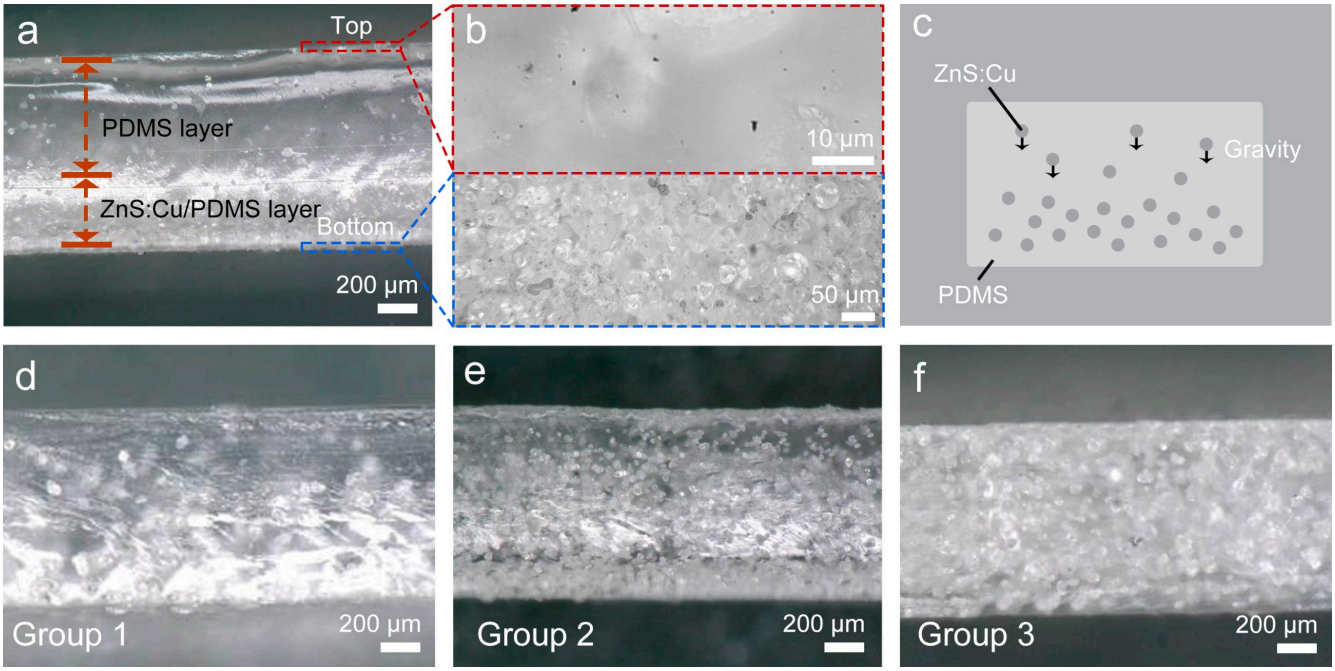


Figure 1. (**a**) Side view, (**b**) top view, and (**c**) bottom view of ZnS:Cu/PDMS coating prepared by method 1 (48 h curing). (**c**) Schematic illustration of stratification phenomenon in the curing process. Side view of ZnS:Cu/PDMS coatings prepared by method 2: (**d**) Group 1, (**e**) Group 2, and (**f**) Group 3.

3.2. Characterization Analysis

The elemental composition of the coating surface was analyzed by XPS (Figure 2a). The peaks at 102.84 eV (Si2p), 153.83 eV (Si2s), 285.13 eV (C1s), and 532.92 eV (O1s) are typical characteristics of PDMS [25]. However, although ZnS:Cu was incorporated into PDMS, no XPS signal was detected in the composite. In the narrow XPS spectrum (Figure 2b,c), the Zn2p and Cu2p signals are close to the background signal, indicating that they can be neglected. Because the SFEs of ZnS:Cu and PDMS differ, the ZnS:Cu particles were completely wrapped in PDMS. In XPS measurements, the probe can only detect a depth of several nanometers, and it is difficult and challenging to measure heterogeneous and layered surfaces [33]; hence, no ZnS:Cu signal was detected in the measurement. In the FT-IR spectra of PDMS and ZnS:Cu/PDMS, the peak at 786.86 cm^{-1} is due to $-CH_3$ rocking and the $\equiv Si-C$ stretch in $\equiv Si-CH_3$, the peak at 1008.89 cm^{-1} is due to $-(CH_2)-$ wagging vibrations, and the peak at 1257.16 cm^{-1} is assigned to symmetric $-CH_3$ deformation. In the FT-IR spectrum of ZnS:Cu (black line in Figure 2d), the peak at 580.48 cm^{-1} is due to the Zn-S vibration. However, no such peaks were detected for PDMS or ZnS:Cu/PDMS. Given that FT-IR is a transmission light measurement technique and that the ZnS:Cu powders are light-tight, the ZnS:Cu signal is too weak to be detected in 1 mm thick ZnS:Cu/PDMS coating. The ZnS:Cu sample prepared using the KBr pellet method was sufficiently thin (tens of microns) for some of the light to pass through; hence, the ZnS:Cu sample showed a Zn-S peak at 580.48 cm^{-1}. The Cu concentration in ZnS:Cu is typically very low [34,35]; therefore, the Cu signal is too weak to be detected by FT-IR measurements. The EDS measurements (Figure 2e) agree with the XPS results, which show no difference in the Cu and Zn contents in the two samples.

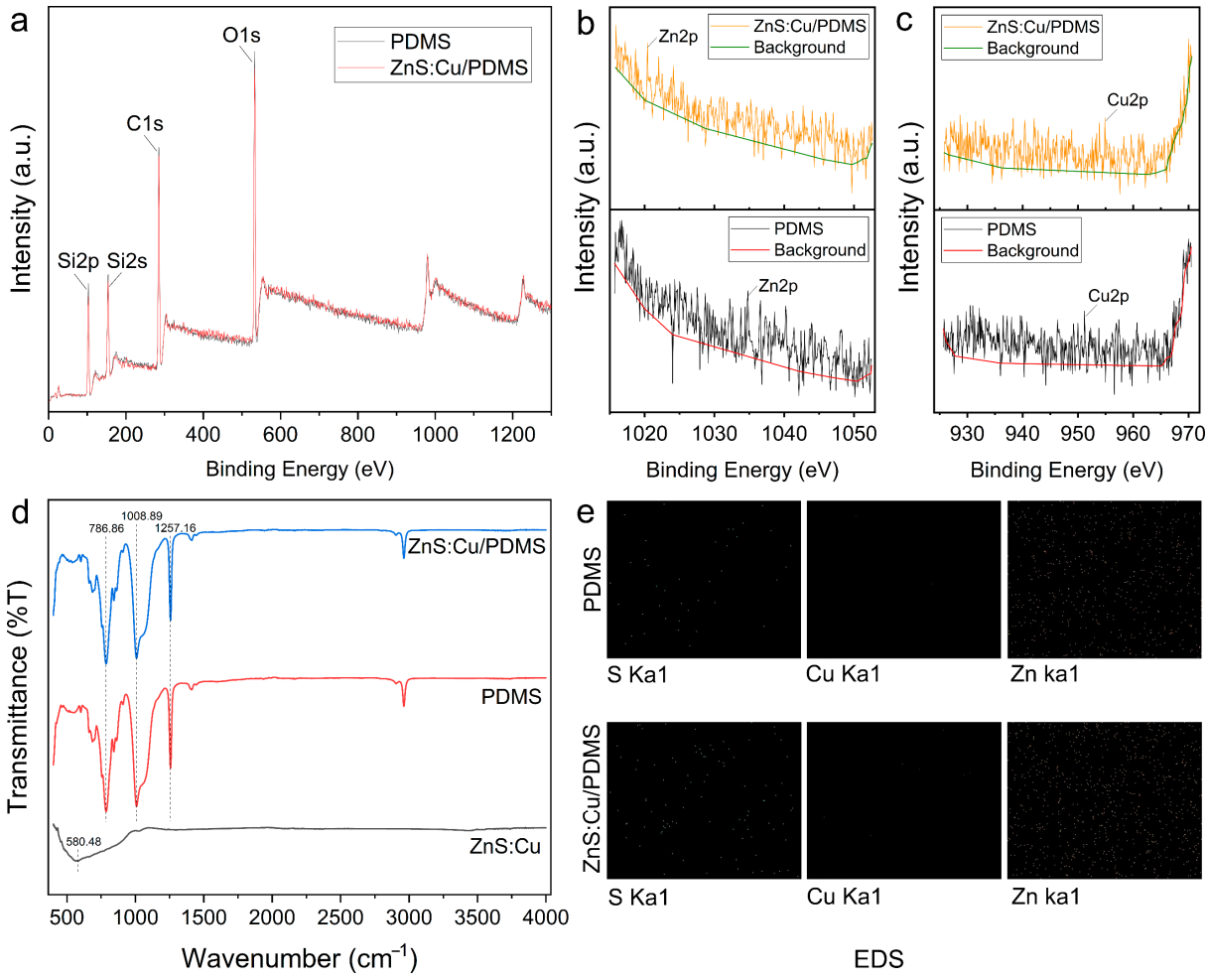


Figure 2. (**a**) XPS survey and (**b**,**c**) narrow spectra of PDMS and ZnS:Cu/PDMS. (**d**) FT-IR spectra of ZnS:Cu, PDMS, and ZnS:Cu/PDMS. (**e**) EDS measurement of PDMS and ZnS:Cu/PDMS.

Surface wettability and SFE are crucial parameters for determining the antifouling capability of coatings [1]. Figure 3a shows that the WCAs of the surfaces ranged from 109.8° to 112.4°, indicating that they were hydrophobic and that the incorporation of ZnS:Cu in the PDMS had no effect on the surface wettability. The SFE values of the coatings were similar, ranging from 15.7 to 17.2 mJ/m^2. According to Baier's curve, a surface exhibits the minimum attachment strength if its SFE ranges from 20 to 25 mJ/m^2 [36]. Although the ZnS:Cu/PDMS coatings have lower SFE values, their SFE range is conducive to combating biofouling.

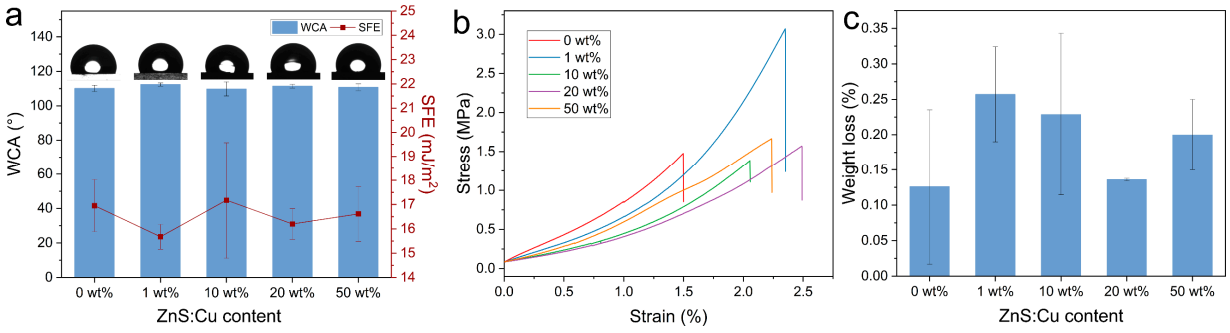


Figure 3. (**a**) WCA and SFE measurements. (**b**) Stress–strain curves of the samples. (**c**) Weight loss in the samples.

Figure 3b shows the results of the tensile tests. The results indicate that the stress–strain curve decreased with increasing ZnS:Cu content. This may have been caused by stress concentration, and the ZnS:Cu particles in the PDMS provided the stress concentration points. However, the stress–strain curve of the 50 wt% sample did not follow the aforementioned trend. This is because excessive ZnS:Cu particles in the PDMS provide sufficient tensile strength, and the effect of the stress concentration becomes weak. We assume that all the samples are subjected to a tensile force of 1 MPa, and a higher strain indicates that the coating is prone to deformation, that is, softer. According to fracture mechanics and tests, the elastic modulus and stiffness of coatings influence the adhesion of fouling organisms [37,38]. Specifically, a low elastic modulus and soft coating are helpful in preventing biofouling adhesion. Hence, the incorporation of ZnS:Cu into PDMS helps combat biofouling.

Figure 3c shows that the weight loss in the 0 wt% sample is 0.13 ± 0.1%, indicating that the pristine PDMS can lose weight in the test procedure. When ZnS:Cu was incorporated into the PDMS, the weight loss in all composite samples increased. This indicates that the ZnS:Cu particles can be released into water. The weight loss in the ZnS:Cu/PDMS coatings decreased with increasing ZnS:Cu content. A possible reason is that the increased ZnS:Cu ratio resulted in enhanced compactness of the composite coatings; thus, the channel for water molecules to enter the composite coatings was narrowed. However, the weight loss in the 50 wt% sample was greater than that of the 20 wt% sample. As excess ZnS:Cu particles were incorporated into the 50 wt% sample, the number of ZnS:Cu particles exposed to water molecules increased.

3.3. Antifouling Tests

Because bacteria and algae are the major contributors to the primary stage of biofouling, antifouling tests against *B. subtilis* and *Chlorella* were performed. *B. subtilis* is commonly found in marine environments [39]. It is a typical rod-shaped bacteria with a length of 2–4 µm (Figure 4a). In the antifouling test against *B. subtilis*, the 1 wt% sample showed an average antibacterial ratio of 25.5% (Figure 4b), and the bacterial colonies on samples are shown in Figure S1. The antibacterial ratio increased to 63.8% when the ZnS:Cu content increased from 1 to 10 wt%. However, when the ZnS:Cu content was increased to 20 wt%, the antibacterial ratio decreased to 52.6%. A possible reason for this is that the ZnS:Cu release rate of the 10 wt% sample was higher than that of the 20 wt% sample (Figure 3c), but the latter was softer than the former (Figure 3b); hence, both effects resulted in the 20 wt% sample exhibiting reduced antifouling capability. The 50 wt% sample had the highest ZnS:Cu content and exhibited the highest antibacterial ratio of 66.4%, indicating its excellent antifouling capability. The possible antibacterial mechanisms of ZnS:Cu can be analyzed based on the antibacterial activities of pristine ZnS and Cu [35]. According to previous reports, the generating of biologically reactive oxygen species (ROS) is the antibacterial mechanism of ZnS. These ROS, such as superoxide anions, hydroxyl ions, and hydroxyl radicals, damage bacterial cells by attacking cytoplasmic and extra-cytoplasmic targets [40]. The Cu ions have multiple antibacterial effects, including ROS generating, protein oxidation, DNA degradation, and lipid peroxidation [41].

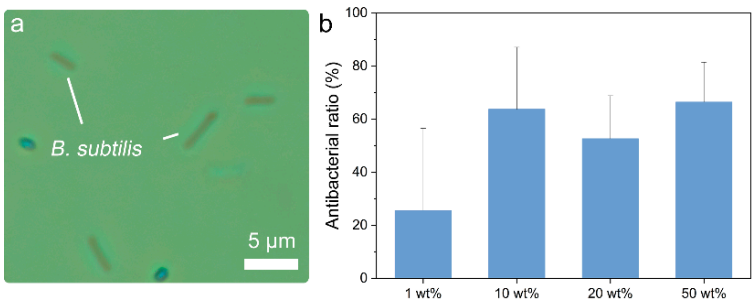


Figure 4. (**a**) Optical microscopic image of *B. subtilis*. (**b**) Antibacterial ratios of the samples.

The antifouling tests against *Chlorella* were conducted under static and dynamic conditions. In the static tests (Figure 5a), many *Chlorella* cells covered the 0 wt% sample. Among the samples with ZnS:Cu contents, the 1 wt% and 10 wt% samples showed several *Chlorella* colonies, whereas the 20 wt% and 50 wt% samples showed only a few scattered *Chlorella* cells. According to the quantized data in Figure 5c, the antifouling capability of the samples increased with increasing ZnS:Cu content. This variation trend was different from that observed in the antibacterial tests, indicating that the ZnS:Cu particles have a selective antifouling capability. In the dynamic tests, the antifouling capability of the samples increased with increasing ZnS:Cu content. The numbers of *Chlorella* cells on the 0 wt%, 1 wt%, and 10 wt% samples were significantly decreased in the dynamic tests (Figure 5b) compared with those in the static tests (Figure 5a), and the numbers of *Chlorella* cells on the 20 wt% and 50 wt% samples showed a reduction to some extent. There are several mechanisms underlying these results in the dynamic tests. First, ZnS:Cu particles may have a high release ratio in flowing water. Second, deformation is more likely to occur on the ZnS:Cu/PDMS surface than on the pristine PDMS under the impact of water flow; thus, fouling organisms can easily detach from the surface during continuous deformation. Thirdly, surface deformation may induce fluorescence to prevent the settlement of *Chlorella*. Hence, the samples exhibited better antifouling capabilities under dynamic conditions than under static conditions. A schematic illustration of the antifouling mechanisms of the ZnS:Cu/PDMS coatings is shown in Figure 5d. According to these tests, the 50 wt% sample exhibited the best antifouling capability. Although coatings with a higher ZnS:Cu content (e.g., 60 wt%) may have better antifouling capabilities, this can lead to a significant increase in costs. Hence, the 50 wt% sample is a good candidate for practical applications.

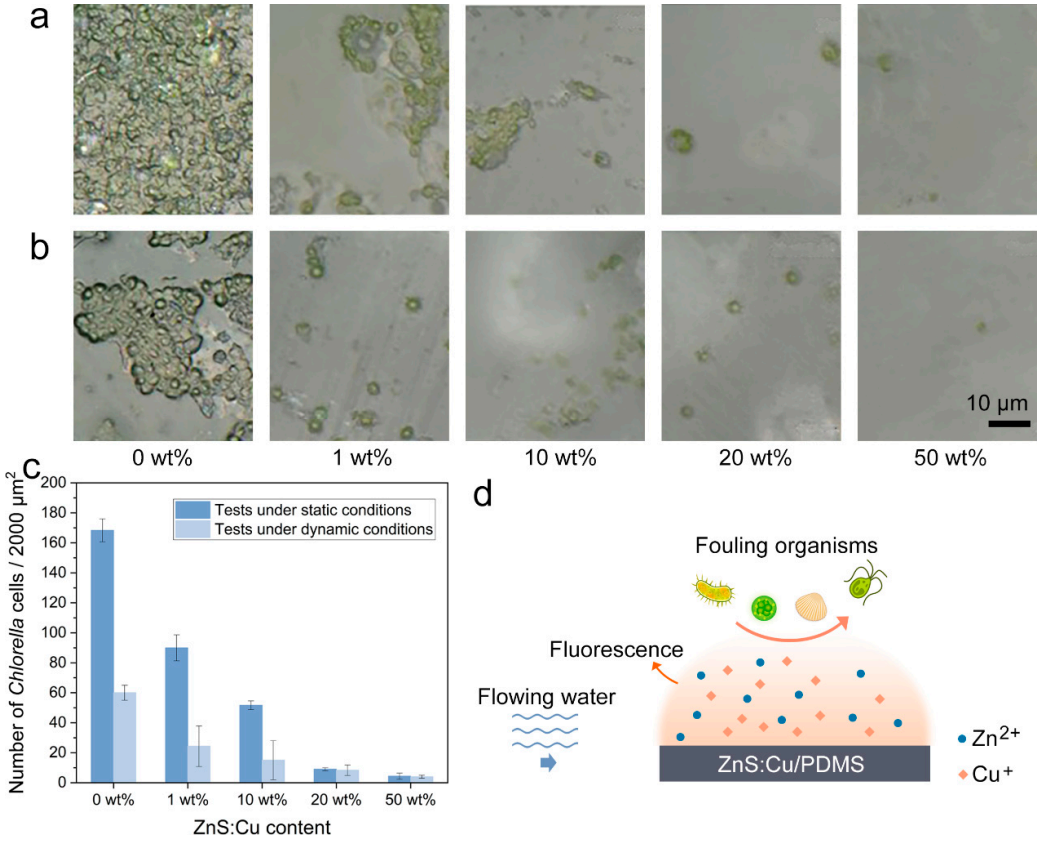


Figure 5. Optical microscopic images of *Chlorella* under (**a**) static conditions and (**b**) dynamic conditions (all the images share the same scale bar). (**c**) Number of settled *Chlorella* cells under static conditions and dynamic conditions. (**d**) Schematic illustration of antifouling mechanisms of ZnS:Cu/PDMS coatings.

4. Conclusions

A series of ZnS:Cu/PDMS coatings with different ZnS:Cu contents was prepared. The preparation method was simple and cost-effective. These coatings exhibited hydrophobicity, which is conducive to combating biofouling. The ZnS:Cu/PDMS coatings exhibited excellent antifouling capabilities against *B. subtilis* and *Chlorella*. Specifically, the 50 wt% sample exhibited the best antifouling capability. The ZnS:Cu/PDMS coatings may prevent biofouling by releasing ions (Zn^{2+} and Cu^{+}), inducing deformation, and emitting fluorescence. In natural marine environments, there are few perfectly still waters and continuous water flows move beneath the water's surface. The 50 wt% ZnS:Cu/PDMS coating is expected to exhibit enhanced antifouling capabilities in natural marine environments. This study provides a reference for the application of Zn^{2+}/Cu^{+} combinations to combat marine biofouling. However, the antifouling capability of the fluorescence emission in this study requires more direct evidence and further study.

Supplementary Materials: The following supporting information can be downloaded at: https://www.mdpi.com/article/10.3390/coatings13122083/s1, Figure S1: Bacterial colonies on the samples.

Author Contributions: Writing—original draft preparation, Z.L. and H.J.; conceptualization, Z.L., W.D. and H.J.; investigation, Z.L., Y.Z. and T.W.; writing—review and editing, W.D. and H.J.; project administration, W.D. and H.J. All authors have read and agreed to the published version of the manuscript.

Funding: This work was supported by the Scientific Research Project of the Education Department of Jilin Province (Grant No. JJKH20241265KJ) and the Key Laboratory Fund of National Defense Science and Technology (Grant No. JCKY61420052009).

Institutional Review Board Statement: Not applicable.

Informed Consent Statement: Not applicable.

Data Availability Statement: Data are contained within the article and supplementary materials.

Conflicts of Interest: The authors declare no conflict of interest.

References

1. Jin, H.; Tian, L.; Bing, W.; Zhao, J.; Ren, L. Bioinspired marine antifouling coatings: Status, prospects, and future. *Prog. Mater. Sci.* **2022**, *124*, 100889. [CrossRef]
2. Jin, H.; Wang, J.; Tian, L.; Gao, M.; Zhao, J.; Ren, L. Recent advances in emerging integrated antifouling and anticorrosion coatings. *Mater. Des.* **2022**, *213*, 110307. [CrossRef]
3. Chen, P.; Chen, J.; Zhang, W.; Tang, L.; Cheng, G.; Li, H.; Fan, T.; Wang, J.; Zhong, W.; Song, Y. Biochemical mechanisms of tributyltin chloride-induced cell toxicity in Sertoli cells. *Ecotoxicol. Environ. Saf.* **2023**, *255*, 114725. [CrossRef]
4. Beyer, J.; Song, Y.; Tollefsen, K.E.; Berge, J.A.; Tveiten, L.; Helland, A.; Øxnevad, S.; Schøyen, M. The ecotoxicology of marine tributyltin (TBT) hotspots: A review. *Mar. Environ. Res.* **2022**, *179*, 105689. [CrossRef] [PubMed]
5. Xie, Q.; Pan, J.; Ma, C.; Zhang, G. Dynamic surface antifouling: Mechanism and systems. *Soft Matter* **2019**, *15*, 1087–1107. [CrossRef]
6. Al-Belushi, M.A.; Myint, M.T.Z.; Kyaw, H.H.; Al-Naamani, L.; Al-Mamari, R.; Al-Abri, M.; Dobretsov, S. ZnO nanorod-chitosan composite coatings with enhanced antifouling properties. *Int. J. Biol. Macromol.* **2020**, *162*, 1743–1751. [CrossRef] [PubMed]
7. Calabrese, C.; La Parola, V.; Testa, M.L.; Liotta, L.F. Antifouling and antimicrobial activity of Ag, Cu and Fe nanoparticles supported on silica and titania. *Inorg. Chim. Acta* **2022**, *529*, 120636. [CrossRef]
8. Ciriminna, R.; Bright, F.V.; Pagliaro, M. Ecofriendly Antifouling Marine Coatings. *ACS Sustain. Chem. Eng.* **2015**, *3*, 559–565. [CrossRef]
9. Ytreberg, E.; Karlsson, J.; Eklund, B. Comparison of toxicity and release rates of Cu and Zn from anti-fouling paints leached in natural and artificial brackish seawater. *Sci. Total Environ.* **2010**, *408*, 2459–2466. [CrossRef]
10. Selim, M.S.; Yang, H.; Wang, F.Q.; Fatthallah, N.A.; Huang, Y.; Kuga, S. Silicone/ZnO nanorod composite coating as a marine antifouling surface. *Appl. Surf. Sci.* **2019**, *466*, 40–50. [CrossRef]
11. Pang, W.Y.; Ahmad, A.L.; Zaulkiflee, N.D. Antifouling and antibacterial evaluation of ZnO/MWCNT dual nanofiller polyethersulfone mixed matrix membrane. *J. Environ. Manag.* **2019**, *249*, 109358. [CrossRef] [PubMed]

12. Sri Abirami Saraswathi, M.S.; Rana, D.; Divya, K.; Gowrishankar, S.; Nagendran, A. Versatility of hydrophilic and antifouling PVDF ultrafiltration membranes tailored with polyhexanide coated copper oxide nanoparticles. *Polym. Test.* **2020**, *84*, 106367. [CrossRef]
13. Mao, T.; Lu, G.; Xu, C.; Yu, H.; Yu, J. Preparation and properties of polyvinylpyrrolidone-cuprous oxide microcapsule antifouling coating. *Prog. Org. Coat.* **2020**, *141*, 105317. [CrossRef]
14. Nastyshyn, S.; Raczkowska, J.; Stetsyshyn, Y.; Orzechowska, B.; Bernasik, A.; Shymborska, Y.; Brzychczy-Włoch, M.; Gosiewski, T.; Lishchynskyi, O.; Ohar, H.; et al. Non-cytotoxic, temperature-responsive and antibacterial POEGMA based nanocomposite coatings with silver nanoparticles. *RSC Adv.* **2020**, *10*, 10155–10166. [CrossRef]
15. Deng, Y.; Song, G.-L.; Zheng, D.; Zhang, Y. Fabrication and synergistic antibacterial and antifouling effect of an organic/inorganic hybrid coating embedded with nanocomposite Ag@TA-SiO_2 particles. *Colloids Surf. A Physicochem. Eng. Asp.* **2021**, *613*, 126085. [CrossRef]
16. Selim, M.S.; El-Safty, S.A.; El-Sockary, M.A.; Hashem, A.I.; Abo Elenien, O.M.; El-Saeed, A.M.; Fatthallah, N.A. Modeling of spherical silver nanoparticles in silicone-based nanocomposites for marine antifouling. *RSC Adv.* **2015**, *5*, 63175–63185. [CrossRef]
17. Miller, R.J.; Adeleye, A.S.; Page, H.M.; Kui, L.; Lenihan, H.S.; Keller, A.A. Nano and traditional copper and zinc antifouling coatings: Metal release and impact on marine sessile invertebrate communities. *J. Nanopart. Res.* **2020**, *22*, 129. [CrossRef]
18. Tian, J.; Xu, K.; Hu, J.; Zhang, S.; Cao, G.; Shao, G. Durable self-polishing antifouling Cu-Ti coating by a micron-scale Cu/Ti laminated microstructure design. *J. Mater. Sci. Technol.* **2021**, *79*, 62–74. [CrossRef]
19. Calabrese, C.; Parola, V.L.; Cappello, S.; Visco, A.; Scolaro, C.; Liotta, L.F. Antifouling Systems Based on Copper and Silver Nanoparticles Supported on Silica, Titania, and Silica/Titania Mixed Oxides. *Nanomaterials* **2022**, *12*, 2371. [CrossRef]
20. Mohan, M.V.K.; Prakash, T.V.K.B.; Mukherjee, A. Antifouling paint formulations with ZnO and Fe_2O_3 nano-paints for marine applications. *Sustain. Chem. Pharm.* **2022**, *30*, 100858. [CrossRef]
21. Soleimani, S.; Jannesari, A.; Yousefzadi, M.; Ghaderi, A.; Shahdadi, A. Eco-friendly foul release coatings based on a novel reduced graphene oxide/Ag nanocomposite prepared by a green synthesis approach. *Prog. Org. Coat.* **2021**, *151*, 106107. [CrossRef]
22. Lv, Y.; Zheng, Y.; Zhu, H.; Wu, Y. Designing a dual-functional material with barrier anti-corrosion and photocatalytic antifouling properties using g-C_3N_4 nanosheet with ZnO nanoring. *J. Mater. Sci. Technol.* **2022**, *106*, 56–69. [CrossRef]
23. Wang, S.; Deng, L.; Lv, Y.; Zhang, T.; Zhang, X.; Dong, Z.; Cai, G. Construction of antifouling Cu-modified TiO_2 coating via micro-arc oxidation: The influence of Cu content. *Surf. Coat. Technol.* **2023**, *454*, 129197. [CrossRef]
24. Sohn, K.-S.; Timilsina, S.; Singh, S.P.; Choi, T.; Kim, J.S. Mechanically driven luminescence in a ZnS:Cu-PDMS composite. *APL Mater.* **2016**, *4*, 106102. [CrossRef]
25. Jin, H.; Bing, W.; Jin, E.; Tian, L.; Jiang, Y. Bioinspired PDMS–Phosphor–Silicone Rubber Sandwich-Structure Coatings for Combating Biofouling. *Adv. Mater. Interfaces* **2020**, *7*, 1901577. [CrossRef]
26. Guo, H.; Song, L.; Hu, J.; Lin, T.; Li, X.; Yu, H.; Cheng, D.; Hou, Y.; Zhan, X.; Zhang, Q. Enhanced antifouling strategy with a strong synergistic effect of fluorescent antifouling and contact bacteriostasis using 7-amino-4-methylcoumarin. *Chem. Eng. J.* **2021**, *420*, 127676. [CrossRef]
27. Xiong, G.; Zhang, Z.; Qi, Y. Effect of the properties of long afterglow phosphors on the antifouling performance of silicone fouling-release coating. *Prog. Org. Coat.* **2022**, *170*, 106965. [CrossRef]
28. Yao, Y.; Wei, Y.; Chen, S. Size effect of the surface energy density of nanoparticles. *Surf. Sci.* **2015**, *636*, 19–24. [CrossRef]
29. Han, B.; Wang, H.; Bing, W.; Jin, H. Bacterial adhesion properties of parylene C and D deposited on polydimethylsiloxane. *New J. Chem.* **2022**, *46*, 8773–8778. [CrossRef]
30. *GB/T 528-2009*; Rubber, Vulcanized or Thermoplastic—Determination of Tensile Stress-Strain Properties. General Administration of Quality Supervision, Inspection and Quarantine of the People's Republic of China: Beijing, China, 2009.
31. Bing, W.; Cai, Y.; Jin, H.; Tian, L.; Tian, L.; Yin, Y.; Teng, Y.; Wang, P.; Hou, Z.; Bai, X. An antiadhesion and antibacterial platform based on parylene F coatings. *Prog. Org. Coat.* **2021**, *151*, 106021. [CrossRef]
32. Chakraborti, R.K.; Kaur, J. Noninvasive Measurement of Particle-Settling Velocity and Comparison with Stokes' Law. *J. Environ. Eng.* **2014**, *140*, 04013008. [CrossRef]
33. Szklarczyk, M.; Macak, K.; Roberts, A.J.; Takahashi, K.; Hutton, S.; Głaszczka, R.; Blomfield, C. Sub-nanometer resolution XPS depth profiling: Sensing of atoms. *Appl. Surf. Sci.* **2017**, *411*, 386–393. [CrossRef]
34. Peng, W.Q.; Cong, G.W.; Qu, S.C.; Wang, Z.G. Synthesis and photoluminescence of ZnS:Cu nanoparticles. *Opt. Mater.* **2006**, *29*, 313–317. [CrossRef]
35. Chaliha, C.; Nath, B.K.; Verma, P.K.; Kalita, E. Synthesis of functionalized Cu:ZnS nanosystems and its antibacterial potential. *Arab. J. Chem.* **2019**, *12*, 515–524. [CrossRef]
36. Selim, M.S.; Shenashen, M.A.; El-Safty, S.A.; Higazy, S.A.; Selim, M.M.; Isago, H.; Elmarakbi, A. Recent progress in marine foul-release polymeric nanocomposite coatings. *Prog. Mater. Sci.* **2017**, *87*, 1–32. [CrossRef]
37. Brady, R.F. A fracture mechanical analysis of fouling release from nontoxic antifouling coatings. *Prog. Org. Coat.* **2001**, *43*, 188–192. [CrossRef]
38. Peng, Q.; Zhou, X.; Wang, Z.; Xie, Q.; Ma, C.; Zhang, G.; Gong, X. Three-Dimensional Bacterial Motions near a Surface Investigated by Digital Holographic Microscopy: Effect of Surface Stiffness. *Langmuir* **2019**, *35*, 12257–12263. [CrossRef]
39. Wang, Y.S.; Liu, L.; Fu, Q.; Sun, J.; An, Z.Y.; Ding, R.; Li, Y.; Zhao, X.D. Effect of *Bacillus subtilis* on corrosion behavior of 10MnNiCrCu steel in marine environment. *Sci. Rep.* **2020**, *10*, 5744. [CrossRef]

40. He, W.; Jia, H.; Cai, J.; Han, X.; Zheng, Z.; Wamer, W.G.; Yin, J.-J. Production of Reactive Oxygen Species and Electrons from Photoexcited ZnO and ZnS Nanoparticles: A Comparative Study for Unraveling their Distinct Photocatalytic Activities. *J. Phys. Chem. C* **2016**, *120*, 3187–3195. [CrossRef]
41. Lv, P.; Zhu, L.; Yu, Y.; Wang, W.; Liu, G.; Lu, H. Effect of NaOH concentration on antibacterial activities of Cu nanoparticles and the antibacterial mechanism. *Mater. Sci. Eng. C* **2020**, *110*, 110669. [CrossRef]

Disclaimer/Publisher's Note: The statements, opinions and data contained in all publications are solely those of the individual author(s) and contributor(s) and not of MDPI and/or the editor(s). MDPI and/or the editor(s) disclaim responsibility for any injury to people or property resulting from any ideas, methods, instructions or products referred to in the content.